Nucleation calculations in a pair-binding model

J. A. Venables

School of Mathematical and Physical Sciences, University of Sussex, Brighton BN1 9QH, Sussex, United Kingdom
and Department of Physics, Arizona State University, Tempe, Arizona 85287
(Received 5 December 1986)

Calculations of the nucleation and growth of thin films are presented. These atomistic calculations depend on adsorption (E_a), diffusion (E_d), and lateral binding (E_b) energies. A simplified pair binding model of small two-dimensional clusters is used to make the calculations explicit for layer-plus-island (or Stranski-Krastanov) growth systems. Within such a model it is found that at least a crude (Einstein) representation of surface vibrations is needed to make reasonable predictions at low supersaturation. The calculations are applied to extract parameter values from nucleation and growth experiments on Ag/W(110), Ag/Mo(100), Ag/Si(111), and Ag/Si(100), and for rare gases onto various (plated) substrates. Comments are made about the parameters obtained for these systems, and about the role of surface crystallography and defects.

I. INTRODUCTION

Nucleation and growth processes are responsible for the structure of thin films grown on surfaces. It is generally accepted that there are three types of growth possible, in the simplest cases when there is no interdiffusion between deposit and substrate. The extensive experimental work which has been done to test our ideas about these processes has been reviewed.[1]

In the much-studied island, or Volmer-Weber, growth mode, small three-dimensional (3D) clusters form directly on the bare substrate. In the layer, or Frank–van der Merwe, growth mode, it is expected that two-dimensional (2D) clusters will form on each layer, provided that the spacing between nuclei is small in comparison to the spacing between steps on the surface.

In the layer-plus-island, or Stanski-Krastanov (SK), growth mode the simplest picture is that the layers form first, and that the islands grow from two- or three-dimensional clusters on top of the intermediate layer(s). This is illustrated schematically in Fig. 1. This figure also points out that the experimental variables are the substrate temperature T and the arrival rate R, and indicates important energy parameters. In practice, it seems that the SK mode is quite close to layer growth, and that the growth of islands can sometimes proceed alongside further layer growth. In this case, it seems reasonable to consider the nuclei to be 2D clusters, with conversion to 3D islands taking place at a later stage.

The purpose of this paper is to present a simplified nucleation theory of 2D clusters which can be applied to layer and SK growth modes. In these modes, the deposits often grow at relatively low supersaturation values, $S = R/R_e$, where R_e is the reevaporation rate of the bulk deposit at the given temperature T. In such conditions the chemical potential driving force for condensation $\Delta\mu = kT \ln S$ is also small. It is shown here that to ensure self-consistency for small S values, explicit account must be taken of surface vibrations. Calculations within the Einstein model are presented to illustrate this

point. These calculations are then used to abstract parameters from both Ag and rare-gas deposition systems. The results for Ag have recently been described in outline, in the context of a recent conference review;[2] here the details needed to understand such results are given and discussed.

The theory is used to make specific predictions for the stable cluster density $n_x(R,T)$ which can then be compared with the experimental (maximum or saturation) island density $N(R,T)$. For complete condensation conditions the predictions depend on diffusion (E_d) and lateral binding (E_b) energies. The onset of incomplete condensation results in a dramatic decrease in $n_x(R,T)$ at a temperature determined in addition by the adsorption energy (E_a). Thus application of this model amounts to the simplest two parameter (or three parameter at high temperatures) fit to the experimental data $N(R,T)$, measured by microscopy.

Particular emphasis is given to the systems Ag/W(110),[3] Ag/Mo(100),[4] and Ag/Si(100) and
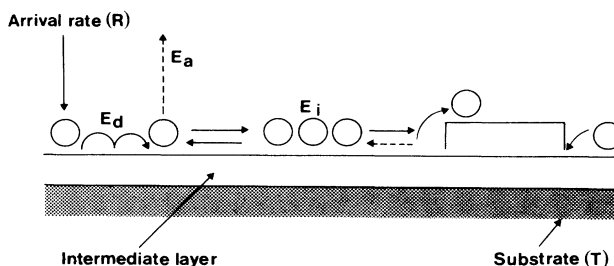

FIG. 1. Schematic illustration of the processes occurring in layer plus island, or Stranski-Krastanov growth. The independent variables are the arrival rate (R) and substrate temperature (T). Also indicated are the activation energies for adsorption (E_a) and diffusion (E_d), and the binding energy E_i of the critical cluster, which contains i atoms. Here and in Fig. 2, the dotted lines indicate the processes which are less important in this growth mode.

Ag/Si(111),[5] which have been studied by using UHV scanning electron microscopy (SEM) techniques. Comments are also made on rare-gas deposition systems, which were studied recently[6] and earlier[7] by low-temperature transmission electron microscopy (TEM) techniques.

The nucleation theory developed previously is described in Sec. II: this is extended to ensure consistency in the low supersaturation limit in Sec. III. Comparisons with experiment are made in Sec. IV: a discussion follows in Sec. V.

II. NUCLEATION OF 2D CLUSTERS

A. Rate equations and processes

The first nucleation theory for 2D clusters was given by Stowell and Hutchinson,[8] and a general equation for the maximum cluster density was first given by Stowell.[9] The nucleation theory needed can be derived within the rate equation framework described previously,[10] assuming single adatoms to be the only species which are effectively mobile on the surface. The equations for the density n_j of clusters of size j can be written as

$$dn_1/dt = R - n_1/\tau_a - d(n_x w_x)/dt \ , \tag{2.1}$$

$$dn_j/dt = 0 \ (2 \le j \le i) \ , \tag{2.2}$$

$$dn_x/dt = \sigma_i D n_1 n_i - 2 n_x \, dZ/dt \ . \tag{2.3}$$

Here Eq. (2.1) expresses the change in single adatom population n_1 due to arrival from the vapor at rate R, loss by evaporation with a stay time τ_a, and by incorporation into existing clusters. Equation (2.2) expresses the (approximate) local thermodynamic equilibrium which exists between subcritical clusters of size $j \le i$. The critical size i corresponds to the clusters with the lowest concentration, or highest free energy if equilibrium is assumed.

Equation (2.3) sums the supercritical (stable) clusters as $n_x = \sum_{j=i+1}^{\infty} n_j$, in terms of a nucleation rate $(\sigma_i D n_1 n_i)$ and a coalescence rate proportional to the rate of change of the substrate coverage by stable clusters (Z).

The coupling of Eqs. (2.1) and (2.3) arises because of the interaction between nucleation and growth stages, as illustrated in Fig. 2.[2] The last term in (2.1) can be written as

$$d(n_x w_x)/dt = n_1/\tau_n + n_1/\tau_c + RZ \ . \tag{2.4}$$

The three terms represent incorporation of single atoms into stable clusters by nucleation, diffusion capture, and direct impingement, respectively. As shown earlier,[1,10] most nucleation occurs under steady-state conditions, with $dn_1/dt = 0$ in Eq. (2.1). Under these conditions it is convenient to write (2.1) and (2.4) as

$$n_1 = R\tau(1 - Z) \ , \tag{2.5}$$

with $\tau^{-1} = \tau_a^{-1} + \tau_n^{-1} + \tau_c^{-1}$, where $\tau_c^{-1} = \sigma_x D n_x$. This expresses the competitive nature of reevaporation, which is dominant at high temperatures, and capture by stable
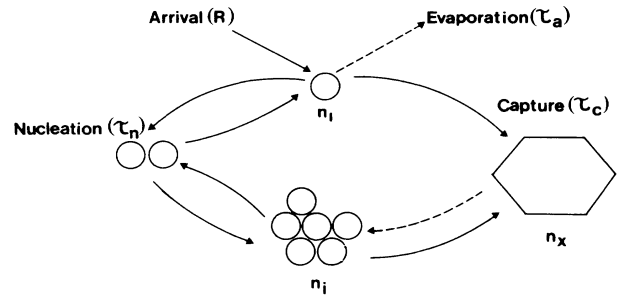

FIG. 2. Schematic illustration of the interaction between the nucleation and growth stages. The single adatom population (n_1) determines the critical cluster population (n_i); however, n_1 is itself determined by the arrival rate R, and the characteristic times for evaporation (τ_a), nucleation (τ_n), and diffusion capture (τ_c) by n_x stable clusters. Only after these clusters cover a sizable fraction of the substrate (Z) is direct impingement significant.

clusters which dominates at low temperatures under complete condensation conditions; the nucleation term is always unimportant numerically, and will be ignored subsequently. The capture number σ_x and the adatom diffusion coefficient D enter via solution of the relevant (2D) diffusion equation.[10]

Two other relations are needed to couple (2.1) and (2.3) analytically. There is first the relation between substrate coverage Z and atoms in stable clusters $(n_x w_x = \sum_{j=i+1}^{\infty} n_j w_j)$. Specializing to 2D clusters, this is simply

$$dZ/dt = N_a^{-1} d(n_x w_x)/dt \ , \tag{2.6}$$

where N_a is the density of atoms per unit area in the deposit. Clearly if the deposit is 1 ML thick, $N_a^{-1} = \Omega^{2/3}$, where Ω is the atomic volume, but Eq. (2.6) allows for (constant thickness) multilayer nuclei.

The second relation needed is that between n_i and n_1 in (local) thermodynamic equilibrium. This is the Walton relation, often written in the form

$$(n_i/N_0) = (n_1/N_0)^i \sum_m C_i(m) \exp[\beta E_i(m)] \ , \tag{2.7}$$

where $N_0 =$ the substrate atomic density, $\beta = (kT)^{-1}$, and $E_i(m)$ and $C_i(m)$ are the energies and statistical weightings of i-sized clusters of configuration m. In simplified theories appropriate to relatively high supersaturation $(S \gg 1)$, Eq. (2.7) is limited to one configuration having the highest binding energy, so that we write C_i and E_i for a given i.

When these (2D) approximations have been made, Eq. (2.3) can be written as a function of the coverage Z, i.e.,

$$dn_x/dZ = J - 2 n_x \ , \tag{2.8}$$

where the "nucleation rate" term is

$$J = (\sigma_i C_i D n_1^{i+1} \exp(\beta E_i) N_0^{1-i} N_a)/(\sigma_x D n_1 n_x + RZ)$$

and n_1 is given by Eq. (2.5). The differential equation (2.8) for $n_x(Z)$ therefore has solutions which depend on

the dominant contribution to n_1. However, Stowell[9] initially showed that the maximum cluster density, assumed to occur at a coverage Z_0, can be obtained simply from Eq. (2.8) as $n_x = J/2$. Rearranging this equation and setting in the explicit expressions for J and n_1 leads eventually to

$$(n_x/N_0)(g+r)^i(Z_0+r) = f(Z_0,i)(R/N_0^2 D)^i$$

$$\times \exp(\beta E_i)(\sigma_x D \tau_a N_0)^{i+1} ,$$

$$(2.9)$$

where the ratio $r = \tau_a/\tau_c = \sigma_x D \tau_a n_x$. Equation (2.9) is of the same form as given previously (Ref. 1, Eq. 2.17), but the constants f, g, and Z_0 contained in Eq. (2.9) have been retained explicitly. This means that the three analytical regimes (denoted *complete, initially incomplete,* and *extreme incomplete*[1]) can be obtained exactly, depending on which terms are dominant on the left-hand side of Eq. (2.9). For complete condensation $r \gg g$, for initially incomplete condensation $Z_0 < r < g$, and for extreme incomplete condensation $r \ll Z_0$.

Equation (2.9) has been used to calculate $n_x(R,T)$ in general, given particular forms for D, τ_a, and E_i. But for layer and Stranski-Krastanov growth, the special case of *complete condensation*, when reevaporation is negligible, is particularly important. In this case, Eq. (2.9) simplifies to

$$(n_x/N_0)^{i+2} = f(Z_0,i)(R/N_0^2 D)^i \exp(\beta E_i) . \quad (2.10)$$

By taking the $(i+2)$th root of this equation we obtain an equation of the same form as derived previously[1,3,5] for (n_x/N_0), with the correct constants. In order to reproduce this regime exactly we have $f(Z_0,i) = \eta(Z_0,i) Q(i)$ with $Q(i) = (\sigma_i C_i N_a/N_0)^{1/(i+2)}$, and $\eta(Z,i)$ as computed previously (Ref. 1, Fig. 6c or Ref. 3, Fig. 5). The factor g is given by $g^i = \sigma_x^{i+1}$. In Eq. (2.9), however, its exact value is unimportant as it is only used to interpolate between the low- and high-temperature regimes, so we have used $\sigma_x = 5$. A short physical argument explaining the form of Eq. (2.10) is given elsewhere.[2] It is also important to realize that (n_x/N_0) is very insensitive to the choice of Z_0 since most nucleation occurs in the low-temperature limit $Z \ll Z_0$.

B. Thermally activated processes and numerical solutions

The various processes: adsorption, adatom diffusion, cluster formation, and bulk evaporation and/or condensation are typically thermally activated processes with Arrhenius temperature dependences, and energies E_a, E_d, and E_i indicated in Fig. 1. In particular, it is conventional to write the adatom stay time τ_a as

$$\tau_a^{-1} = v_a \exp(-\beta E_a) \quad (2.11)$$

and the diffusion constant D as

$$D = \alpha v_d N_0^{-1} \exp(-\beta E_d) , \quad (2.12)$$

where E_a, v_a and E_d, v_d are adsorption and diffusion energies and frequencies, respectively, and $\alpha = 0.25$ for

diffusion in two dimensions.

Evaluation of the right-hand side of Eq. (2.9) or (2.10) requires a model for the critical cluster binding energy E_i. In fact only models in which all E_j can be evaluated can be solved. This is because these equations *assume* that i is the critical size, and correspondingly that local equilibrium is maintained [Eq. (2.7)] for all $j \leq i$. This only happens for small j, and the actual critical size i is that size for which $n_x(j)$, or equivalently the predicted nucleation rate $J(j)$, is a minimum.[1] Thus this paper is limited to a very specific pair binding model in which $E_j = b_j E_b$, and b_j is the number of nearest-neighbor bonds, of strength E_b, in a j-sized cluster. Furthermore, the explicit calculations have to assume a particular cluster geometry. Although any geometry is possible in principle, and is of course actually determined by the forces between the adatoms themselves and the substrate, we assume here close-packed clusters on a hexagonal lattice. For these, the b_j can be evaluated by simple counting, and some values are given in Appendix A.

With these values Eq. (2.10) can be solved directly. Equation (2.9) is solved by iteration, using Eq. (2.10) as the starting point. In this complete condensation limit, the $n_x(R,T)$ predictions depend sensitively on E_d [via Eq. (2.12)] and E_b, and less on the frequency factor v_d and numerical constants. Such predictions have been published previously for Ag/W(110).[11] When reevaporation is allowed [Eq. (2.9)], the behavior at high temperatures is also influenced sensitively by E_a. Some calculations for Ag/Si(111) and (100) using Eq. (2.11) inserted into (2.9) have been published.[5] However, these high-temperature predictions need to be revised as discussed in the next section.

III. NUCLEATION AT LOW SUPERSATURATION

A. General considerations

It might seem an elementary requirement that a nucleation model predicts zero nucleation rate at the equilibrium sublimation pressure p_0 of the deposit: however, this is not assured by the equations described as yet. There are several reasons for this. First, the adsorption energy E_a is a free parameter, which can be used to model adsorption on a substrate different from the deposit material. In this case, as discussed in general terms elsewhere,[1] the effective supersaturation ratio $S = p/p_e$ or R/R_e, where the equilibrium pressure (p_e), or rate of evaporation (R_e), corresponds to a step in the adsorption isotherm, which for layer-growth systems occurs at $p_e < p_0$. For deposition of a material on itself we must have E_a and E_i related to the sublimation energy L by

$$L = E_a + \lim_{i \to \infty} (E_i/i) . \quad (3.1)$$

For a special case of a lattice with nearest neighbor pair bonds this reduces to $L = E_a + b_\infty E_b$, and for the hexagonal lattice $b_\infty = 3$.

In this limit of large critical cluster size we can see that the transition to incomplete condensation will take place approximately when Eq. (2.10), for large i, corre-

sponds also to $r = \sigma_x D \tau_a n_x \simeq 1$. By eliminating $\sigma_x D n_x$ we find this condition to be

$$\tau_a^{-1} = v_a \exp(-\beta E_a) = (1 - Z)(R/N_0)\exp(\beta E_i/i) , \quad (3.2)$$

or rearranging using Eq. (3.1):

$$(R/N_0 v_a) = (1 - Z)^{-1}\exp(-\beta L) . \quad (3.3)$$

Equation (3.3) qualitatively follows the sublimation line with energy L, but quantitatively it almost certainly does not. In particular, a finite nucleation rate can still occur within the model at the experimental sublimation pressure, given particular choices of parameters, and Eq. (3.3) does not necessarily describe a line which occurs within the actual crystal-growth regime.

To overcome these problems at low supersaturation, generalizations to Eqs. (2.7) and (2.11) have been made which ensure consistency with the equilibrium sublimation pressure, within an Einstein model of the solid. This model has been used to fit the experimental sublimation pressure quite accurately for the cases of Ag and various rare gases, as described in Appendix B.

Similar arguments could be advanced to change the form of the diffusion constant D [Eq. (2.12)]. But because diffusion is only involved in the kinetics of crystal growth, not the thermodynamics, this has not been done here. In practice the form of the diffusion constant is rather uncertain, and comparison with experiments may have to average over the effects of anisotropic surface crystallography, steps and other defects. Thus we prefer to use E_d in (2.12) as a parameter to characterize the effective value of D which is appropriate to the experiments. This is discussed further in Sec. V.

B. An Einstein model of adsorption, cluster formation, and evaporation

The model considered can be visualized in terms of the vibrations of the entities indicated in Fig. 2. Adsorption of single adatoms is taken to be localized on N_0 sites. In these sites the adatoms vibrate with frequency v_a perpendicular, and v_d parallel to the surface. The corresponding "Einstein" free energy can be expressed in terms of $x_a = h v_a / kT$ and x_d using the function we designate as $\mathscr{E}(x)$:

$$\mathscr{E}(x) = 0.5x + \ln[1 - \exp(-x)] ,$$

as

$$E_a(T) = E_a(0) - kT[\mathscr{E}(x_a) + 2\mathscr{E}(x_d)] , \quad (3.4)$$

where $E_a(0)$ corresponds to the energy E_a used previously in Eq. (2.11).

Adsorption in this model follows the Langmuir isotherm for low adatom concentrations n_1, and the equilibrium evaporation rate R_e is given by[12]

$$R_e = p_e / (2\pi m kT)^{1/2}$$

$$= (2\pi m / h^3)(kT)^2 (n_1/N_0)\exp[-\beta E_a(T)] . \quad (3.5)$$

The same model can give the evaporation rate of the bulk solid, with no vacancies, in the form

$$R_e = (2\pi m / h^3)(kT)^2 \exp[-\beta L(T)] , \quad (3.6)$$

where $L(T) = E_a(T) + b_\infty E_b(T)$ is the temperature-dependent sublimation energy corresponding to Eq. (3.1). For consistency, we need $R_e = n_1 / \tau_a$, so that

$$\tau_a^{-1} = (2\pi m / h^3 N_0)(kT)^2 \exp[-\beta E_a(T)] \quad (3.7)$$

is the expression to use instead of Eq. (2.11).

Within the nearest-neighbor model we assume that atoms within clusters on the surface retain the same v_a as isolated adatoms, but have $v_b \neq v_d$ parallel to the surface. This is consistent with Eq. (3.6) provided that

$$E_b(T) = E_b(0) - (2/b_\infty)kT[\mathscr{E}(x_b) - \mathscr{E}(x_d)] , \quad (3.8)$$

where $E_b(0)$ is the E_b used previously. Under these conditions, the cluster free energy $E_j = b_j E_b(T)$ in the simplified Walton expression for $j = i$:

$$(n_i/N_0) = C_i(n_1/N_0)^i \exp[\beta E_i(T)] . \quad (3.9)$$

The above equations [(3.7)–(3.9)] are sufficient to ensure consistency within an Einstein model with the equilibrium vapor pressure of a solid bound by nearest-neighbor forces. Over a limited temperature range p_e (or R_e) can be expressed as

$$p_e = p_0 \exp(-\beta L_0) . \quad (3.10)$$

The values of the parameters L_0 and the average frequency $[(v_a + 2v_b)/3]$ needed to agree with the vapor pressure of bulk Ag and rare gases in the pressure range below 10^{-3} Torr are given in Appendix B.

IV. COMPARISON WITH EXPERIMENT

Recent experimental work at Sussex has involved nucleation and growth studies of Ag on W(110), Mo(100), and Si(100) and Si(111) substrates[3-5] by ultrahigh vacuum SEM. In addition, attempts have been made to grow Xe crystals on (xenon-plated) amorphous carbon substrates at low supersaturation[6] following earlier work at low temperatures and pressures,[7] using TEM techniques. The fit of these experiments to the equations of Secs. II and III are discussed here. The calculations were done and the figures produced on a laboratory based PDP11-23 system.[13]

A. Silver deposits on metals and semiconductors

Figure 3 shows a comparison of the Ag/W(110) $N(T)$ data[3] with the calculated $n_x(T)$ based on the complete condensation equation (2.10). Two curves which fit the data tolerably well are shown, corresponding to different values of E_b around 0.3 eV and E_d around 0.1 eV. The larger value of E_d (0.15 eV) gives the steeper slope on the Arrhenius plot and vice versa, and corresponds to the smaller values of E_b (0.275 eV). Changes of E_d by around ± 0.05 eV coupled with changes in E_b by 0.025 eV are thus consistent with the data, but much larger changes would be inconsistent. In particular $E_d \geq 0$, so that we can bracket $0 \leq E_d \leq 0.20$ eV, and consequently $0.35 \geq E_b \geq 0.25$ eV.

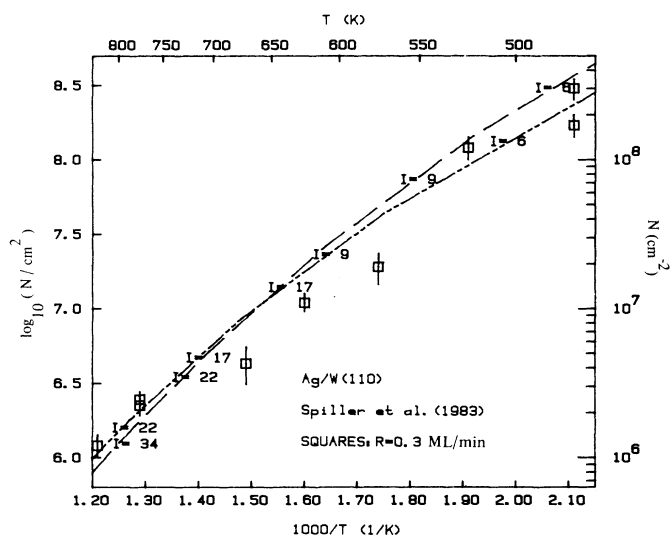Figure 4 shows a similar calculation compared with

FIG. 3. Complete condensation calculation of the nucleation density $N(T)$ for Ag/W(110) with $E_b = 0.275$, $E_d = 0.15$ eV (dashed line), $E_b = 0.325$, $E_d = 0.05$ (dotted-dashed line). The calculated critical nucleus sizes ($I = 17$, etc.) are indicated for each straight line section of the curve, in this and all subsequent figures. Comparison with data (squares) at $R = 0.3$ ML/min from Ref. 3. 1 ML$= 1.38 \times 10^{15}$ atoms cm^{-2}.

the rate-dependence data $N(R)$ for Ag/W(110) at temperatures $T = 573$ and 773 K. The solid lines show the calculation for $E_b = 0.30$ and $E_d = 0.10$ eV, which agree well at the higher temperature, and have the correct slope, if not the exact position, at the lower temperature. Also shown is the curve for $E_d = 0.05$ eV at the lower temperature, which reduces the predicted n_x value by a
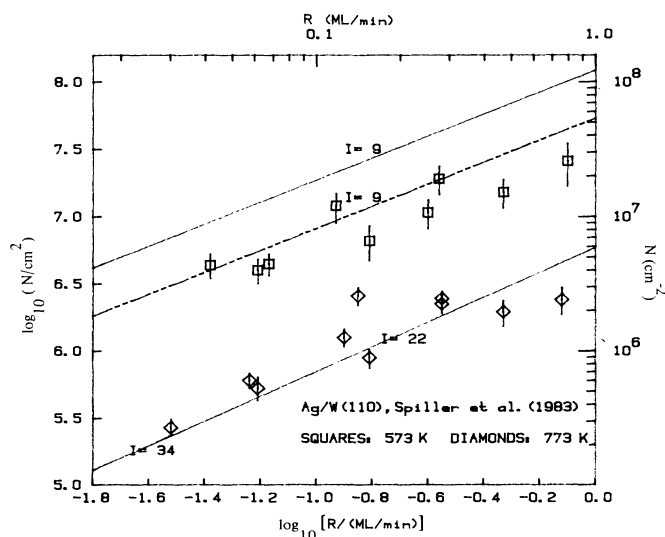
factor of about 2. Both the $N(T)$ and $N(R)$ data fall below the predicted curves in the region of T around 573 K in a manner which is consistent with a critical nucleus size $i \simeq 9$ persisting over a larger region than predicted in this simple model.

The sensitivity of the calculation of $n_x(T)$ to parameter values has been explored within the more general model based on Eq. (2.9), incorporating Einstein vibrations as described in Sec. III B. Unless otherwise stated, the Ag vibration frequencies v_a, v_b, and v_d were all taken equal to 4×10^{12} Hz.[14] Figure 4 was actually produced with this program, but the results agree exactly with the more general program in the complete condensation regime for $v_b = v_d$.

Figure 5 shows the calculation for Ag/W(110) as a function of E_d and E_a for $E_b = 0.30$ eV. In the complete concentration regime, the predicted $n_x(T)$ is sensitive to E_d (0.05–0.15 eV, as illustrated), but independent of E_a provided it is high enough. At the highest temperatures, when condensation goes incomplete, there is a very rapid fall, which depends on E_a, and to a lesser extent on E_d. The highest-temperature values can thus be used to estimate, or at least give a lower limit to E_a. The two values illustrated, 2.05 and 2.15 eV, bracket the highest-temperature data points. It is of course significant that if $E_a \simeq 2.1$ eV and $E_b = 0.3$ eV, the sublimation energy of Ag islands will be $L = E_a + 3E_b \simeq 3.0$ eV, which is very close to the actual sublimation energy for bulk Ag $= 2.95$ eV. This agreement is obtained via the considerations discussed in Sec. III and Appendix B.

Figures 6 and 7 explore the use of the same equations in comparison with data for Ag/Mo(100) (Ref. 4) and Ag/Si(100) (Ref. 5). It is assumed that the nucleating
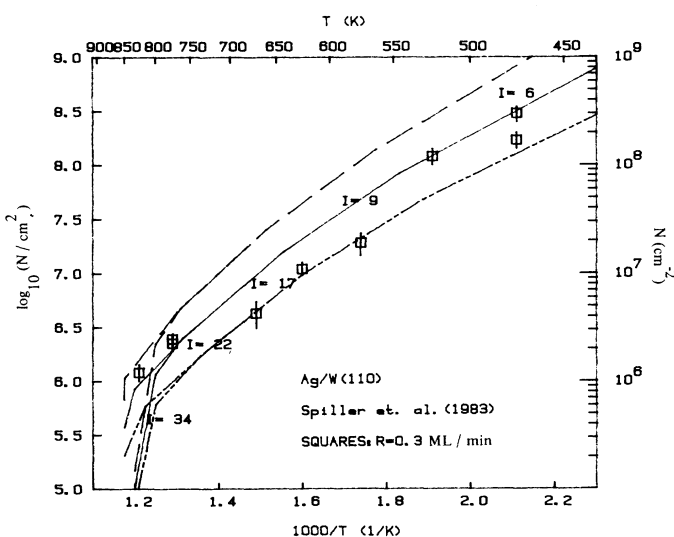

FIG. 4. Calculation of the rate dependence $N(R)$ for Ag/W(110) with $E = 0.30$, $E_d = 0.10$ eV (solid lines), and $E_d = 0.05$ eV (dotted-dashed line). Upper curves and data (squares) at $T = 573$ K, and lower curve and data (diamonds) at 773 K. Data taken from Ref. 3.

FIG. 5. Calculation of the temperature dependence $N(T)$ for Ag/W(110) with $E_b = 0.30$, $E_d = 0.15$ eV (upper dashed line), 0.10 eV (solid line) and 0.05 eV (lower dotted-dashed line). Two curves are superimposed for each of these values, which diverge only at the highest temperatures, corresponding to $E_a = 2.05$ and 2.15 eV.
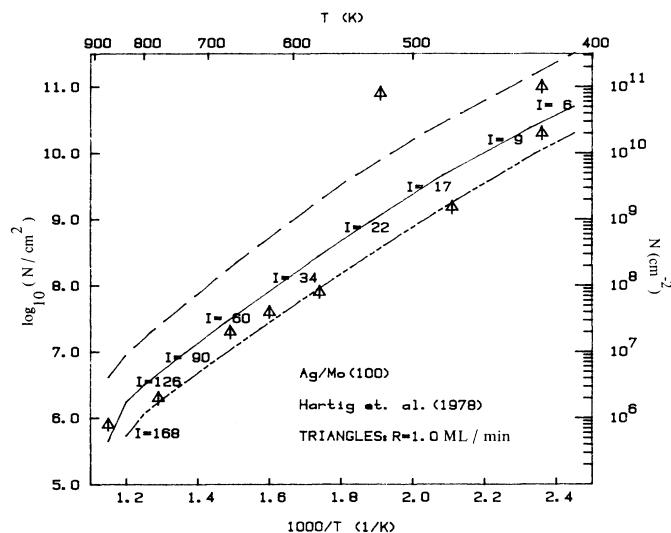
FIG. 6. Calculation of $N(T)$ for Ag/Mo(100) with $E_a = 2.5$, $E_d = 0.45$ eV, and $E_b = 0.175$ eV (upper dashed line), 0.15 (solid line) and 0.125 eV (lower dotted-dashed line). Comparison with data at $R = 1.0$ ML/min from Ref. 4; 1 ML$= 1.2 \times 10^{15}$ atoms cm^{-2}.

FIG. 7. Calculation of $N(T)$ for Ag/Si(100) with $E_a = 2.6$, $E_b = 0.1$, and $E_d = 0.7$ eV, exploring variations in frequency factors v_a, v_b, and v_d, all of which are 4×10^{12} Hz unless stated otherwise. Upper solid line and data (squares) at $R = 2.0$ ML/min, lower solid line and data (diamonds) at $R = 0.4$ ML/min; data taken from Ref. 5, with 1 ML$= 6.8 \times 10^{14}$ atoms cm^{-2}. Other lines all at $R = 2.0$ ML/min; $v_d = 8 \times 10^{12}$ Hz (upper dashed line), 2×10^{12} Hz (lower dotted-dashed line); $v_a = 8 \times 10^{12}$ Hz (long-dashed line, at highest temperatures only).

clusters have hexagonal geometry, which is undoubtedly incorrect in detail. Thus values deduced for E_b in particular are effective values. Given, however, the extreme sensitivity of the predictions to E_b and E_d, the results put tight limits on the possibilities open for more detailed models.

The Ag/Mo(100) $N(T)$ data (Fig. 6) shows a steeper temperature dependence than the Ag/W(110) data. This is consistent with a larger diffusion energy E_d and smaller binding energy E_b; the curve for $E_d = 0.45$ eV and $E_b = 0.15$ eV fits well over a large temperature range. The other curves illustrate the sensitivity to E_b, with $E_b = 0.125$ and 0.175 eV as shown. A similar range of fits is obtained if E_b is fixed at 0.15 eV, and E_d is varied from 0.5 to 0.4 eV. At the highest temperatures the value of E_a is important with $E_a = 2.5$ eV illustrated. Again the highest-temperature data point needs $E_a \geq 2.5$ eV and $E_a + 3E_b \geq 2.95$ eV as required for the comparison with bulk Ag. The larger critical nucleus sizes, $6 \leq i \leq 168$ in the temperature range illustrated, arise from the smaller E_b value.

The same trend is apparent in the Ag/Si(100) comparison of Fig. 7. The solid lines are the fits to $E_d = 0.7$ eV and $E_b = 0.1$ eV, with $E_a = 2.6$ eV. Although the data are somewhat scattered, the fits can only be made with small-E_b and high-E_d values. Essentially similar curves were published earlier,[5] but without the incorporation of Einstein vibrations; such a model, based on Eq. (2.11), needed $E_a = 2.1$ eV to fit the data. This relatively large shift of 0.5 eV arises via the high pre-exponential factor (up to 8×10^{16} Hz) implied by Eq. (3.7). Again $E_a + 3E_b$ is essentially consistent with bulk Ag sublimation if $E_a \simeq 2.6$ eV, but not if $E_a = 2.1$ eV.
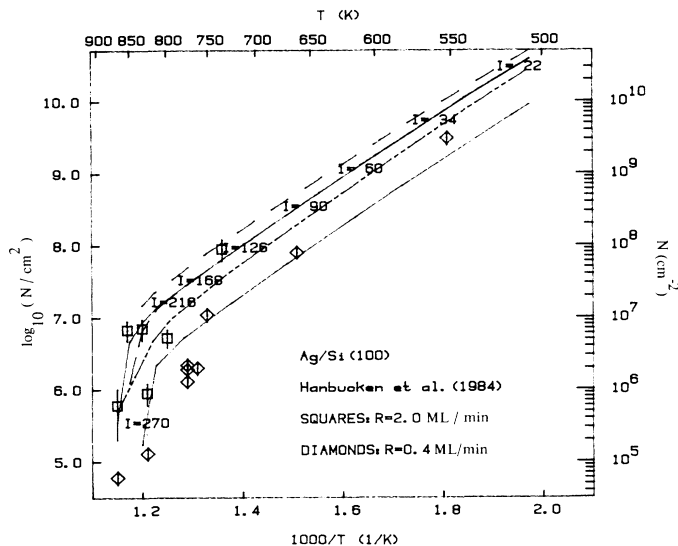
Figure 7 also shows, for the higher rate calculations, the sensitivity of the results to changes of factors of 2 in v_a, v_b, and v_d. In the complete condensation regime, increasing v_d raises $n_x(T)$ and vice versa. This is the result of two opposing tendencies: increasing D in Eqs. (2.10) and increasing $E_i(T)$ in Eq. (3.9); the second is more important and so n_x increases slightly. Increasing v_a decreases $n_x(T)$ at the highest temperatures via the decrease in τ_a in Eq. (3.7). However, none of these effects are very drastic, and do not markedly affect predicted nucleation densities.

Predictions of $n_x(T)$ for Ag/Si(111) have been published previously (Ref. 5, Fig. 8). The above calculations also reproduce this figure provided $E_a = 2.6$ eV rather than 2.1 eV. The comparison with experimental data for this system clearly shows the effect of surface preparation treatment, in that less well-prepared substrates produce higher nucleation densities. In this case, the difference between two sets of experiments could be accounted for by having $E_d \simeq 0.33$ and 0.55 eV on the better and worse substrates, respectively, while E_b remained at 0.1 eV.

It is clear in this case, and maybe by extension to others, that the E_d values deduced are effective values which are constrained by the assumed form of $D(T)$ given by Eq. (2.12); The actual value of $D(T)$ could have different E_d and pre-exponential factors which cannot be disentangled from a comparison only with $N(T)$ values; nonetheless the absolute values of $D(T)$ must be close to the value given by inserting the deduced E_d values into

Eq. (2.12), with $v_d = 4 \times 10^{12}$ Hz and N_0 equal to the monolayer density for the system considered.

It is worth noting that, in the complete condensation regime with large i values, changes in $D(T)$ due to defects in the substrate are more effective in changing $n_x(T)$ than changes in E_i. This is because D (and E_d) appear to the power $-i/(i+2)$, whereas E_i appear to the $+1/(i+2)$th power in Eq. (2.10). Thus defect densities and defect binding (via D^{-1}) affect n_x almost linearly; but if the effect on E_i is limited to a few of the i atoms, only the average $E_i/(i+2)$ intervenes. Thus the occasional high experimental points on the plots (Fig. 6, for example) may be ascribed to a low effective D due to the defects; it is of course impossible to say that such effects are entirely absent in the other cases. The above reasoning is not valid for incomplete condensation, where the effect of defect binding on increasing the population of single adatoms and small clusters is dominant; but the complete condensation regime is much more important in the Stranski-Krastanov cases considered.

B. Rare-gas deposits on amorphous carbon

The nucleation and growth of rare-gas crystals has been extensively studied. The earlier work[7] has since been shown[15] to be incorrect as a description of the nucleation of xenon on clean graphite, which follows the layer-growth mode; however, the results are substantially correct as a description of xenon growth on various xenon-plated substrates including "dirty" graphite, amorphous carbon, or plastic specimen supports such as

pioloform. Similar, but more qualitative experiments have been carried out recently, at higher temperature close to the sublimation line, in an attempt to grow better Xe and Kr crystals.[6]

The analysis of rare-gas crystal growth is interesting partly because pair-binding models are a reasonable starting point, and partly because the experimental results span an extremely wide range of conditions. Also the experimental conditions where islands are observed correspond to Stranski-Krastanov growth, with the intermediate layer in the form of a more or less regular adsorbed gas layer.

In the case of Xe condensed onto dirty graphite, there was evidence (Ref. 7, Fig. 10), from delay times for the appearance of crystals, that the intermediate layer was ~ 1 ML thick; from subsequent studies (e.g., Ref. 16), it is clear that this will depend sensitively on the gas-substrate combination and on the substrate condition. However, the rapid drop in adsorption energy in the first few layers[17,18] towards the value for bulk (xenon) ensures that the effective intermediate layer is quite like a (111) plane of the bulk deposit, with, however, a higher roughness, which we can parametrize via E_d, while keeping E_b appropriate to the bulk deposit.

The fit of Eq. (2.9) to the earlier data,[7] with E_b fixed in this way, and E_d and E_a free parameters, is shown for Xe and Kr in Fig. 8 and Ar in Fig. 9. The quality of the fits is discussed in the next section.

Once condensation becomes incomplete the exact values of both the nucleation rate and the nucleation density are extremely sensitive to the parameters used.
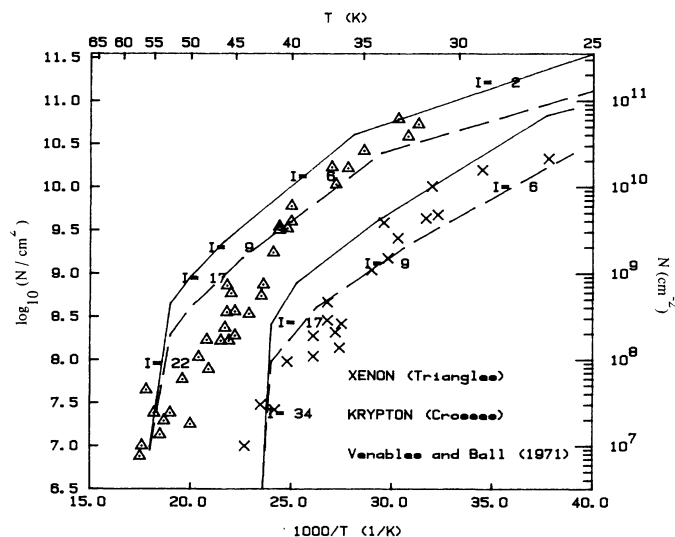

FIG. 8. Calculation of $N(T)$ for Xe and Kr crystals using constants E_b and N_0 from Table II, and $v_a = v_b = v_d$ from Table IV. For Xe, $E_a = 1400$ K, $E_d = 250$ K (solid line) and 200 K (dashed line); the data are the triangles. For Kr, $E_a = 1100$ K, $E_d = 200$ K (solid line) and 150 K (dashed line) with data as crosses. Data from Ref. 7 for an effective pressure p at the substrate of 3×10^{-5} Torr.
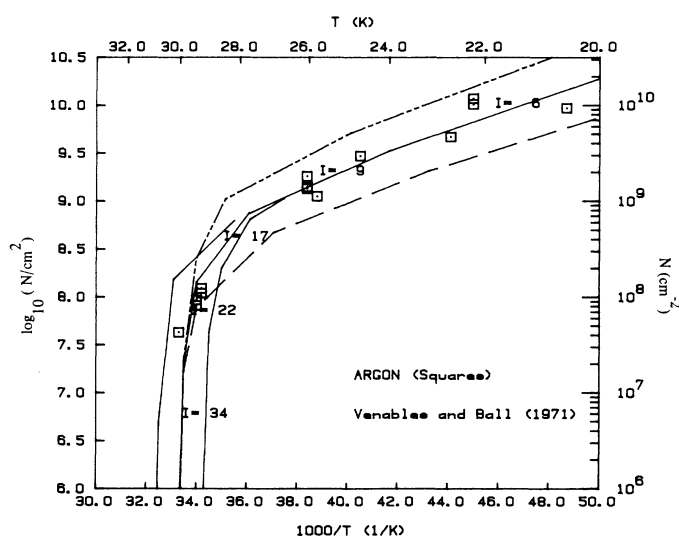
FIG. 9. Calculation of $N(T)$ for Ar crystals analogous to Fig. 8. Curves shown for $E_a = 700$, 725, and 750 K with $E_d = 100$ K (solid lines); $E_a = 725$ K with $E_d = 125$ K (upper dotted-dashed line) and $E_a = 75$ K (lower dashed line). Data from Ref. 7 as squares for an effective pressure p at the substrate of 5×10^{-5} Torr.

However, with the same parameters it was possible to predict the effective onset of nucleation at low supersaturation $(1.1 \leq S \leq 1.2)$ with very low nucleation densities $(n_x \sim 10^2$ cm$^{-2})$, to correspond qualitatively with recent experiments at high pressures $(p \sim 50$ Torr, or $R \geq 10^8$ ML/min.[6] These tests are not very sensitive to the value of E_d used, but are very sensitive to agreement of E_a, E_b and ν_a with the bulk sublimation line, and with the correct constants, as discussed in Sec. III and Appendix B.

V. DISCUSSION AND CONCLUSIONS

The calculations presented can be considered to give a good qualitative description of nucleation and growth processes in the Stranski-Krastanov growth mode. They can be interpreted quantitatively as a two parameter $(E_b$ and $E_d)$ fit to experiments in the complete condensation regime. In addition the fit at the highest temperatures is sensitive to E_a, and the simple Einstein model presented in Sec. III ensures self-consistency in this regime. It is thus practical, within the limitations imposed by the simplified model, to extract these parameters and correlate them with other known features of the deposition systems studied experimentally, most obviously the structure and lattice parameter of the intermediate layer. This is attempted for the silver deposition systems in Table I.

The low-E_d and high-E_b values for Ag/W(110) are associated with the intermediate layer being very close to the (111) plane of bulk Ag, both in structure and lattice parameter. Nonetheless the value of $E_b \simeq 0.3$ eV is low, considerably less than the value $L/6 = 0.492$ eV which would be appropriate for an isotropically bonded surface. Corresponding $E_a \simeq 2.1$ eV is considerably greater than $L/2$, which is the value for a nearest-neighbor model of a (111) surface. This clearly reflects the non-pair additive nature of metallic bonding. It is interesting that Kolaczkiewicz and Bauer[19] have found similar values for E_b from a thermodynamic analysis of this Ag/W(110) system. The strong lack of pair additivity is also seen in the binding energy of isolated Ag$_2$ and Ag$_3$ molecules, 1.65 and 2.62 eV, respectively.[20]

The values for Ag/Mo(100) imply higher $E_d \simeq 0.45$ eV and lower $E_b \simeq 0.15$ eV. This may be rationalized in terms of the more open structure of the (100) surface, the slightly larger lattice parameter (lower N_0), and the fact that the (100)-oriented intermediate layer will inhibit the

formation of compact hexagonal clusters. In fact the islands grow in a (100) orientation also, so the value of E_b is only an effective value, which is a suitable average of nearest- and next-nearest-neighbor bond strengths. In order to get condensation at all at the highest temperatures we must have $E_a \geq 2.5$ eV. This value of $E_a \simeq 0.85L$ is again greater than $0.67L$ which is appropriate to a nearest-neighbor model of the (100) surface.

The Ag/Si(100) and Ag/Si(111) cases have very low E_b values ≤ 0.1 eV and E_d values ranging upwards from ~ 0.33 eV for well-prepared (111) surfaces to ~ 0.7 eV for (100). The monolayer density is only about half that of bulk silver, and this, in addition to the surface reconstructions must be very effective in keeping the diffusing Ag atoms apart. This leads to large critical nucleus sizes, and, it is presumed, to fluidlike nuclei. On the (100) surface there is clearly competition between at least two epitaxial orientations for the islands,[21] and the diffusion coefficient may well be anisotropic due to the 2×1 reconstruction; on the (111) surface, defects clearly strongly influence D. Consequently the values are effective values and should not be overinterpreted. Nonetheless, the adsorption energy E_a has to be high $(\sim 2.6$ eV) in both cases. This value is certainly of interest as a test of metal-semiconductor binding theories.

Thus, the silver deposition systems studied illustrate cases where the lateral binding energy (E_b) is attractive, but substantially reduced with respect to bulk values. The adsorption energy (E_a) is strongly attractive, and higher values are correlated with low E_b values. The effective diffusion energy (E_d) can be correlated with the known orientation, reconstruction, and lattice parameter of the intermediate layers: (100) surfaces have higher E_d values than (111) surfaces, and reconstruction increases E_d, at least in the four systems studied as yet.

More qualitative conclusions can be drawn from a reexamination of experiments on rare-gas growth on amorphous carbon and similar substrates. Whereas Xe, Kr, and Ar grown on clean graphite are archetypical examples of layer growth, impurities or surface irregularities convert these to Stranski-Krastanov growth systems. The values of E_d and E_a needed to agree with experiments[7] are given in Table II, on the assumption that the lateral pair binding energy E_b is not reduced from the bulk value. The E_d values are higher than those expected for the (111) plane of the corresponding rare-gas solid, but are still a sufficiently small fraction of E_a to

TABLE I. Silver deposition system parameters.

Substrate	N_0 $(10^{15}$ cm$^{-2})$	Layer thickness	Island orientation	E_b (eV)	E_d (eV)	E_a (eV)
W(110) Ref. 3	1.38	2–3	(111)	0.3	0.1	2.1
Mo(100) Ref. 4	1.20	1–2	(100)	0.15	0.45	2.5
Si(100) Refs. 5 and 21	0.69	1/4	(100) and (210)	0.1	0.7	2.6
Si(111) Ref. 5	0.79	2/3	(111)	0.1	0.33–0.55	2.6

NUCLEATION CALCULATIONS IN A PAIR-BINDING MODEL

TABLE II. Rare-gas deposition parameters. Energies in K/atom.

Gas	N_0 $(10^{15}$ cm$^{-2})$	E_b	E_a (on 1 ML)	E_d (111)	E_a	E_d (range)
Xe	0.610	228	1307	86	1400	125–225
Kr	0.718	164	898	81	1100	100–200
Ar	0.813	119	660	73	725	75–125
	Ref. 22		Ref. 16		This work	

seem reasonable. From the shape of the curves shown in Fig. 8 particularly, it can be seen that a range of E_d is needed to fit the Kr and Xe data. The value of E_d decreases with increasing temperature in the range indicated in Table II. This is what is expected for diffusion over a rough surface. For example, if the diffusing adatoms encounter a mixture of (111)- and (100)-oriented patches, an effective diffusion energy up to some fraction of E_b higher than the (111) value, which decreases with increasing temperature, would be reasonable, and this is observed.

The E_a values needed to fit these experiments are also somewhat higher than for a (111) rare-gas layer, while remaining much less than that calculated for clean graphite. Again this is reasonable for rough rare-gas surfaces. However, these values should not be overinterpreted, since the actual deposition rate R at high temperatures was almost certainly higher than that assumed in the calculation, because of the lack of complete condensation on the walls of the sample holder.

There are clearly some remaining uncertainties in the details of the cluster models, and of the surface diffusion mechanisms. For example, even within the Einstein model there is scope for taking account of the variation of the frequencies within clusters as a function of coordination number,[23] or for using alternative expressions for the diffusion constant. It seems likely that more than a three-parameter fit (E_b, E_d, E_a) risks overinterpretation of the nucleation density $N(R, T)$ on its own. More detailed correlations with related kinetic and thermodynamic measurements can, however, be envisaged, including thermal desorption[14] and work function[19] measurements. We are presently investigating nucleation

TABLE III. Values of j and b_j used for the model studied in this paper.

j	b_j
1	0
2	1
6	9
9	16
17	36
22	49
34	81
60	153
90	237
126	339
168	459
216	597
270	753

densities, size and spatial distributions, and surface diffusion on finite sized deposits[24,25] and consider it likely that such experiments will yield further constraints on detailed models. Such checks should further advance our understanding of the atomic processes of surface diffusion and crystal growth in simple systems.

ACKNOWLEDGMENTS

APPENDIX A: PAIR BINDING IN 2D HEXAGONAL CLUSTERS

The smallest clusters, size j, and the number of bonds per cluster, b_j, can be evaluated by simple drawing and counting. This has been done for the first 37 clusters, and the nucleation programs run with this list. Examination of the output and the list revealed a sequence of two- and three-bond additions (Δb_j) for each atom addition $(\Delta j = 1)$. The only clusters to become critical nuclei for $j > 2$, on the criterion of minimum nucleation density or nucleation rate, were those which followed a step $\Delta b_j = 2$, and preceded a step $\Delta b_{j+1} = 3$: i.e., those whose next size up was particularly stable.

For larger clusters the picture clearly merges with a 2D continuum model. This was approximated by counting the bonds in clusters consisting of n hexagonal shells plus a central atom, and assuming the critical size to consist of one atom less than this. In this model $j = 3n(n+1)$, and $b_j = 3n(3n+1) - 3$ for $n \geq 1$.

TABLE IV. Values of L_0 and v_a needed to agree with the vapor pressure of bulk Ag and rare gases in the pressure range below 10^{-3} Torr.

Material	L_0 (eV)	v_a $(10^{12}$ Hz)
Ag	2.95	4.0
	L_0 (K/atom)[a]	v_a $(10^{12}$ Hz)
Xe	1937	0.73
Kr	1394	0.84
Ar	981	1.02

[a] 11 604 K/atom = 1 eV; this unit is used to facilitate comparison with other work on rare-gas adsorption.

This list used for the illustrations is given in Table III. The list can be further extended by use of the formulas given beyond $n = 9$. Small changes in j or b_j for large sizes do not influence the results unduly.

APPENDIX B: SUBLIMATION PRESSURES WITHIN THE EINSTEIN MODEL

A simplified Einstein model of the vapor pressures of monatomic solids was given by Salter.[26] Neglecting va-cancy and anharmonic effects the formulas reduce to that given in Eq. (3.6). The values of L_0 and v_a needed to agree with experimental data for Xe, Kr, and Ar are discussed by Crawford.[27] For Ag, similar agreement (to a few percent) can be obtained with the same equation with L_0 and v_a values given by LeLay, Manneville, and Kern,[14] based on vapor-pressure measurements by Honig,[28] and their own thermal desorption measurements on Ag crystallites. The values are given in Table IV.

[1] J. A. Venables, G. D. T. Spiller, and M. Hanbücken, Rep. Prog. Phys. 47, 399 (1984).

[2] J. A. Venables, J. Vac. Sci. Technol. B 4, 870 (1986).

[3] G. D. T. Spiller, P. Akhter, and J. A. Venables, Surf. Sci. 131, 517 (1983).

[4] K. Hartig, A. P. Janssen, and J. A. Venables, Surf. Sci. 74, 69 (1978).

[5] M. Hanbücken, M. Futamoto, and J. A. Venables, Surf. Sci. 147, 433 (1984).

[6] R. J. Keyse and J. A. Venables, J. Cryst. Growth 71, 525 (1985).

[7] J. A. Venables and D. J. Ball, Proc. R. Soc. London, Ser. A 322, 331 (1971).

[8] M. J. Stowell and T. E. Hutchinson, Thin Solid Films 8, 41 (1971).

[9] M. J. Stowell, Philos. Mag. 26, 361 (1972).

[10] J. A. Venables, Philos. Mag. 27, 693 (1973).

[11] J. A. Venables, Vacuum 33, 701 (1983); 5th International Conference on Solid Surfaces, Madrid, Spain, 1983 [Vacuum 35(1), 26 (1985)].

[12] J. G. Dash, Films on Solid Surfaces (Academic, New York, 1975), p. 95.

[13] C. J. Harland and J. A. Venables, Ultramicroscopy 17, 9 (1985).

[14] G. Le Lay, M. Manneville, and R. Kern, Surf. Sci. 72, 405 (1978).

[15] G. L. Price and J. A. Venables, Surf. Sci. 49, 264 (1975).

[16] J. A. Venables, J. L. Seguin, J. Suzanne, and M. Bienfait, Surf. Sci. 145, 345 (1984).

[17] G. L. Price, Surf. Sci. 46, 697 (1974).

[18] W. A. Steele, Surf. Sci. 36, 317 (1973).

[19] J. Kolaczkiewicz and E. Bauer, Surf. Sci. 151, 333 (1985).

[20] K. A. Gringerich, I. Shim, S. K. Gupta, and J. E. Kingcade, Surf. Sci. 156, 495 (1985), Table 5.

[21] O. Osasona and J. A. Venables (unpublished); J. A. Venables, J. Vac. Sci. Technol. A4, 762 (1986).

[22] Data from Rare Gas Solids, edited by M. L. Klein and J. A. Venables (Academic, New York, 1976), Vol. I, assuming an all-neighbor Lennard-Jones potential (E_b) and bulk (111) surfaces (N_0).

[23] F. F. Abraham and J. V. Dave, J. Chem. Phys. 55, 1587 (1971).

[24] M. Hanbücken, T. Doust, O. Osasona, G. Le Lay, and J. A. Venables, Surf. Sci. 168, 133 (1986), and unpublished.

[25] G. W. Jones and J. A. Venables, Ultramicroscopy 18, 439 (1985), and unpublished.

[26] L. S. Salter, Trans. Faraday Soc. 59, 657 (1963).

[27] R. K. Crawford, in Rare Gas Solids, edited by M. L. Klein and J. A. Venables (Academic, New York, 1977), Chap. 11, p. 722.

[28] R. E Honig, RCA Rev. 23, 507 (1962).